Published OnlineFirst May 9, 2012; DOI: 10.1158/0008-5472.CAN-12-0277

The T-cell Receptor Repertoire of Tumor-Infiltrating Regulatory T Lymphocytes Is Skewed Toward Public Sequences

Alexander Sainz-Perez[1,2], Annick Lim[1], Brigitte Lemercier[1], and Claude Leclerc[1,2]

Abstract

The accumulation of $CD4^+$ T regulatory cells (Treg) in tumor tissue is a widely described phenomenon in mouse models and in human cancer patients. Understanding the mechanisms by which Treg migrate and accumulate in tumors is important because they strongly influence the potential efficacy of many immunotherapies. In this study, we used immunoscope technology to analyze the T-cell receptor (TCR) repertoire of tumor-infiltrating T cells in non-TCR transgenic mice. Both tumor-infiltrating Tregs and T effector cells (Teff) displayed sequence profiles in the CDR3 region that were characteristic of biased repertoires seen during clonal cell expansions, implying that strong T-cell responses have occurred within the tumor tissue. By comparing the TCR sequences of tumor-infiltrating Tregs, we obtained evidence of the presence of so-called public TCR sequences that are common to many individuals yet were tumor-specific in nature. Such comparisons also suggested that the Treg–Teff conversion process is not an active process at the tumor site or tumor-draining lymph nodes. Our findings strongly suggest that Treg infiltration of tumor tissue is followed by marked proliferation of a few dominant T-cell clones in the tumor. *Cancer Res; 72(14); 3557–69. ©2012 AACR.*

Introduction

$CD4^+$ regulatory T cells (Treg) are characterized by the expression of interleukin-2 (IL-2) receptor alpha chain (CD25; ref. 1) and the forkhead box P3 (Foxp3) transcription factor (2, 3). Numerous studies have shown the central role of Tregs in inducing and maintaining peripheral tolerance through various suppression mechanisms (4, 5). There is also increasing evidence that Tregs control adaptive immune responses induced by bacteria, viruses, and parasites (6), as well as in cancer immunity (7).

Although the exact function and contribution of Tregs to tumor immunity remains controversial, their accumulation in tumor tissue is a widely described phenomenon in mouse models and in human cancer patients (8, 9). Nevertheless, the mechanisms governing this process are poorly understood. One recent study (10) proposed that the rapid recruitment of Tregs and/or expansion into tumors is a consequence of early tumor-cell recognition by memory Tregs specific to self-antigens. Indeed, Tregs have been shown to express a self-reactive TCR repertoire (11), though it is unclear whether the recruitment and activation of Tregs are nonspecifically induced by the tumor environment or specifically triggered by tumor or self-antigens. The accumulation of Treg in tumors could also result from the conversion of peripheral $Foxp3^-$ T-cells into $Foxp3^+$ T-cells, a process that has already been described in the gut, requiring TGF-β and retinoic acid (12, 13).

To address this issue, we used the immunoscope technology to analyze the T-cell receptor (TCR) repertoire of $CD4^+$ T cells infiltrating tumors (14) in non-TCR transgenic Foxp3-GFP knockin mice bearing TC-1 large solid tumors. Tumor-infiltrating and tumor-draining lymph node (dLN) Tregs and effector T cells (Teffs) were purified, submitted to complementarity-determining region 3 (CDR3) spectratype analysis, and compared with cell populations in peripheral lymph nodes (pLN) or spleen from naive mice. We showed marked alterations in CDR3 length distributions for all of the BV chain families analyzed in Treg and Teff samples from every tumor, which strongly suggests clonal expansion of intratumoral T cells. Moreover, we showed the existence of public sequences shared by all TC-1 tumor-infiltrating Treg samples in 6 independent experiments. These results were also confirmed in another tumor model, MO-5. The public sequences were completely different between the 2 tumor models and were not shared by tumor-infiltrating Teff cells, suggesting that the conversion process is not actively contributing to Treg enrichment of the tumor. This study shows that the TCR repertoire of tumor Tregs in non-TCR transgenic mice is skewed toward public sequences and that Tregs infiltrate tumor tissue through an antigen-driven mechanism that is specific to each tumor model and different from that in Teff cells.

Authors' Affiliations: [1]Institut Pasteur, Immune Regulation and Vaccinology Unit, Department of Immunology; and [2]Inserm, U1041, Paris, France

Note: Supplementary data for this article are available at Cancer Research Online (http://cancerres.aacrjournals.org/).

Corresponding Author: Claude Leclerc, Unité de Régulation Immunitaire et Vaccinologie, Institut Pasteur, 25-28 Rue du Dr Roux, 75724 Paris Cedex 15, France. Phone: 33-1-45-68-86-18; Fax: 33-1-45-68-85-40; E-mail: claude.leclerc@pasteur.fr

doi: 10.1158/0008-5472.CAN-12-0277

Published OnlineFirst May 9, 2012; DOI: 10.1158/0008-5472.CAN-12-0277

Materials and Methods

Mice and tumors

Six- to 8-week-old female Foxp3-GFP knockin mice on C57BL/6 background were kindly donated by B. Malissen (Centre d'Immunologie de Marseille-Luminy, Marseille, France) (15). Animals were kept under specific pathogen-free conditions at the Pasteur Institute animal facility with water and food *ad libitum*. All *in vivo* experiments were conducted according to the institutional guidelines for animal care.

TC-1 tumor cells expressing HPV16-E6 and HPV16-E7 proteins and derived from primary mouse lung epithelial cells were obtained from the American Type Culture Collection (LGC Promochem; ref. 16). MO-5 cells, derived from the murine melanoma B16 (OVA transfected) were kindly provided by L. Sigal (University of Massachusetts, Worcester, MA). Tumor cells (1×10^6 TC-1 cells) in 200 μL PBS were injected into the shaved back (right side) of Foxp3-GFP mice. Tumor size, presented as the average of 2 perpendicular diameters (millimeters), was measured at regular intervals with a digital caliper (Mitutoyo).

Cell isolation

pLN (maxillary, axillary, and inguinal) or inguinal tumor-dLN from naive mice were harvested, mechanically disrupted, and filtered to obtain single-cell suspensions. Spleens were harvested and treated for 45 minutes with 400 U/mL collagenase D and 50 μg/mL DNase I (Boehringer Mannheim), dissociated, and filtered to obtain single-cell suspensions. Tumors were harvested, cut into small pieces, and dissociated using the GentleMacs dissociator programs Spleen-01 and Spleen-04.

Flow cytometry analysis

Cell suspensions were first incubated with rat anti-CD16/32 monoclonal antibodies (mAbs; 2.4G2) to block binding to Fc receptors before staining with diverse fluorescent dye–conjugated mAbs. mAbs used for staining were phycoerythrin-conjugated anti-CD69 (HI.2F) and anti-CD44, PerCP-conjugated anti-CD4 (RM4-5) and anti-CD8, Pacific blue–conjugated anti-CD3, Alexa-780–conjugated anti-CD45.2 and allophycocyanin-conjugated anti-CD62L (MEL-14). Cell viability was determined by 7AAD staining. $Foxp3^+$ cells were detected either by testing for eGFP expression or with intracellular staining with anti-Foxp3 mAb (FJK-16), in accordance with the manufacturers' protocol (eBioscience). All mAbs were purchased from BD Pharmingen or eBioscience. Cells were acquired on a CyAn (Coultronics) flow cytometer and analyzed by use of FlowJo (Tree Star) software.

Purification of Teff and Treg cells

Lymph nodes, spleens, and tumor-cell suspensions from Foxp3-GFP knockin mice were incubated with anti-CD4–coated magnetic beads (N418 clone; Miltenyi Biotec) according to the manufacturers' instructions. Phycoerythrin-conjugated anti-CD4 and allophycocyanin-conjugated anti-CD11c were added 10 minutes before the end of the incubation time. After incubation, cells were washed and $CD4^+$ cells were selected on an automated magnetic cell sorter (AutoMACS; Miltenyi Biotec) using the possels program. Positive fractions, composed of 80% to 95% $CD4^+$ cells were further sorted into $CD4^+$Foxp3-GFP^- effector T cells or $CD4^+$Foxp3-GFP^+ Treg cells on a Moflo cell-sorter cytometer (Beckman-Coulter). The purity for each cell type was at least 90%.

Quantitative repertoire analysis of BV repertoires

Total RNA was extracted from highly purified sorted cell samples, using RNeasy Plus MicroKit (Qiagen). First-strand cDNA synthesis was carried out using oligo-dT and RNase H-reverse transcriptase SuperScript II (Invitrogen). Quantitative analysis was carried out as previously described (17, 18) and as detailed in Supplementary Methods. For immunoscope profiles, products were then subjected to run-off reactions with a nested fluorescent primer specific for the constant region for 3 cycles (see in Supplementary Methods). Fluorescence intensities were plotted in arbitrary units on the y-axis, and CDR3 lengths (determined in amino acids) were plotted on the x-axis (14).

Quantitative analysis

For each BV TCR family, the immunoscope profile was quantified using the same methodology as described in Gorochov (19). Briefly, the fraction of the area under each CDR3 length pic, for a specific BV TCR family, was calculated for each sample that was analyzed. Immunoscope profile quantifications from naive spleen samples were used as a control. The extent of perturbation of every CDR3 length pic in a given BV TCR family was calculated by the distance between the analyzed sample and the control. This measure of perturbation was plotted as landscapes obtained with Excel software (Microsoft Corporation).

Cloning and sequencing of CDR3 regions

Total BV8.1/BC- or BV6/BC-amplified products from different cDNA were cloned using the Zero Blunt TOPO PCR Cloning Kit for Sequencing (Invitrogen). Direct sequencing was carried out as previously described (20) and as detailed in Supplementary Methods. Sequences were analyzed using Taps1.1 software (21). V-D-J junction analysis was done using IMGT/JunctionAnalysis tool (22), available at IMGT web site (23).

Statistical analysis

Prism software (GraphPad Software, Inc.) was used to calculate statistical significance for the differences of particular measurements between groups. Two-tailed unpaired *t* test and one-way ANOVA were used; *P* values less than 0.05 were considered to be statistically significant.

Results

TC-1 tumor tissue is infiltrated by a high ratio of activated Treg cells

Twenty-five days after grafting TC-1 cells to Foxp3-GFP mice, we analyzed Tregs in tumor, dLN, and spleen tissues (Supplementary Figs. S1 and S2). A heterogeneous mixture of

Published OnlineFirst May 9, 2012; DOI: 10.1158/0008-5472.CAN-12-0277

various cell types was obtained from tumor tissue with $CD45^+$ $CD3^+$ T cells accounted for less than 10% of these cells from which half were $CD4^+$ (Fig. 1). Tregs represented 60% of tumor-infiltrating $CD4^+$ T cells (Fig. 1D), which confirmed our previous observations on wild-type C57BL/6 TC-1 tumor-bearing mice (24).

Phenotype analysis identified a drastic downregulation of CD62L expression and a significant upregulation of CD44 and CD69 molecules on tumor Treg cells, compared with splenic and LN populations (Fig. 1E and F) associated with increased PD1 expression (data not shown). Tumor-infiltrating Tregs therefore showed phenotypic characteristics of activated T cells.

Tumor Treg cells present biased immunoscope profiles

One possible hypothesis to explain the activated status of tumor Treg cells could be that infiltration into tumor tissue occurred after activation following recognition of tumor-associated antigens (TAA) in the dLN. Alternatively, Treg cells could be attracted to the tumor tissue by the inflammatory environment through a nonantigen-dependent process. Finally, accumulation of Treg in tumors could result from the conversion of tumor-infiltrating effector $CD4^+$ T cells into Foxp3-expressing cells because of the high levels of TGF-β present in tumor tissue. To address these questions, we carried out a complete analysis of the beta chain (BV) TCR repertoire of Treg cells using the immunoscope technology (14) on Tregs

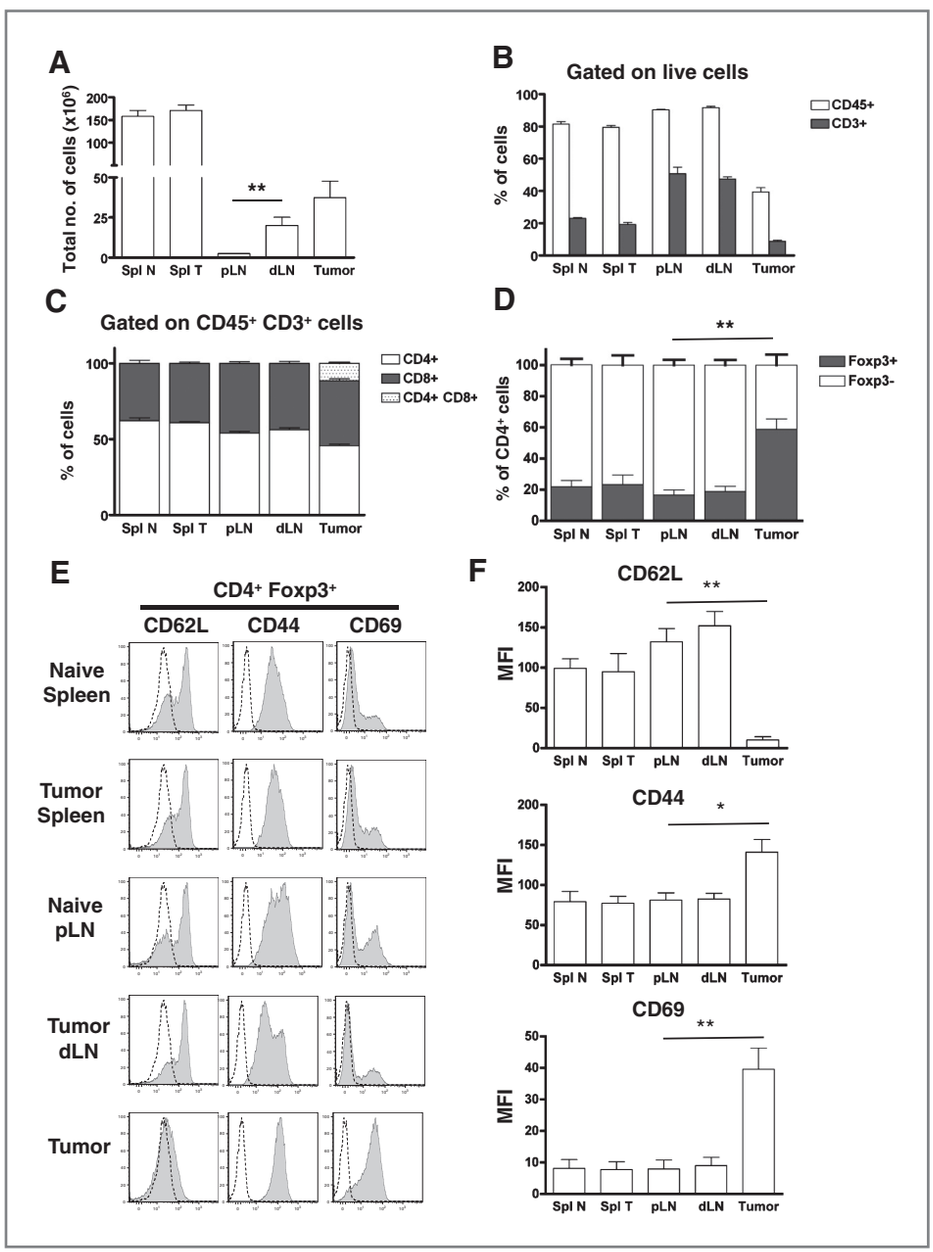

Figure 1. T-cell infiltration of TC-1 tumors is characterized by a high percentage of activated Treg cells. Foxp3-GFP mice were injected on day 0 with 1×10^6 TC-1 cells and 25 days later, mice were killed and spleens (Spl T), tumor-dLNs, and tumors were processed to obtain cell suspensions, which were counted, stained, and analyzed by flow cytometry. Spleens (Spl N) and pLNs from naive Foxp3-GFP mice were identically processed and used as controls. A, total number (mean ± SD) of live cells obtained per organ. B, percentage (mean ± SD) of leukocytes ($CD45^+$) and total T cells ($CD3^+$) among live cells. C, percentage (mean ± SD) among total $CD3^+$ population of $CD4^+$ and $CD8^+$ T cells. D, percentage (mean ± SD) of $CD45^+CD3^+CD4^+$ cells expressing Foxp3 after FACS analysis, gated on live cells. E, surface expression of CD62L, CD44, and CD69 molecules on $CD4^+$ Foxp3-GFP^+ Treg cells. Labelings with isotype control mAbs are represented with dashed lines. One representative experiment of 3 is depicted. F, MFI ± SD of CD62L, CD44, and CD69 expression on $CD4^+$ Foxp3-GFP^+ Treg cells. Results represent pooled data from 3 independent experiments, $n = 5$ (Spl N and Spl T), $n = 7$ (pLN, dLN and tumor). *, $P < 0.05$; **, $P < 0.01$: as determined by one-way ANOVA. FACS, fluorescence-activated cell sorting.

Published OnlineFirst May 9, 2012; DOI: 10.1158/0008-5472.CAN-12-0277

purified from either normal or tumor-bearing mice. The purity of $CD4^+$ Foxp3-GFP$^+$ Tregs and $CD4^+$ Foxp3-GFP$^-$ Teffs was controlled both by flow cytometry (Supplementary Fig. S3) and by real-time PCR analysis of *Foxp3* gene expression (Supplementary Fig. S4). The comparison of CDR3 length profiles was done on samples obtained with the same number of Treg cells to avoid repertoire distortions resulting from the size of samples.

The CDR3 profiles of the BV families obtained from splenic Treg samples from naive mice showed a typical bell-shaped distribution of 6 to 8 distinct CDR3 peaks ranging from 6 to 12-aa in length (Fig. 2A). Such Gaussian distributions are typical of a highly diverse repertoire and reflect a lack of clonal expansion. Each BV family was expressed by a percentage of Treg cells ranging from less than 0.1% to more than 15% (BV-16; Supplementary Fig. S5A). Five different BV families

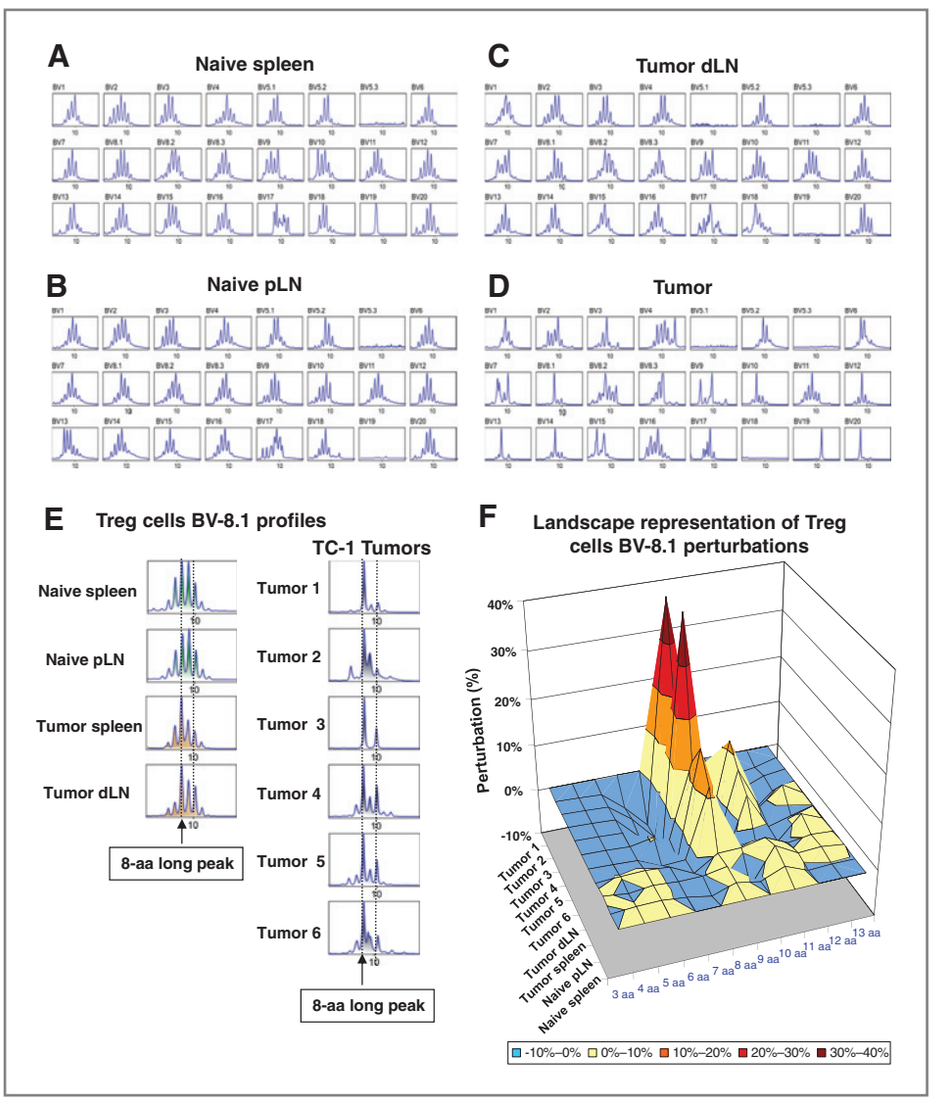

Figure 2. Quantitative spectratyping analysis of the CDR3 length profiles reveals clonal expansions in TC-1 tumor-infiltrating Treg cells. Foxp3-GFP mice were injected on day 0 with 1×10^6 TC-1 cells. Twenty-five days later, mice were killed and spleens, tumor-dLNs, and tumors were processed to obtain cell suspensions. After AutoMacs $CD4^+$ cell enrichment, Foxp3-GFP$^+$ Treg cells were FACS sorted, and total RNA was purified and reverse transcribed. The corresponding cDNA material was then subject to quantitative PCR with primers specific to each BV family and the resulting products were subjected to run-off reactions to obtain immunoscope profiles. Spleens and pLNs from naive Foxp3-GFP mice were identically processed and used as controls. CDR3 length profiles obtained from naive spleen (1.5×10^5 cells; A), naive pLN (1.5×10^5 cells; B), tumor dLN (1.4×10^5 cells; C), and tumor (1.4×10^5 cells, sample 1; D) are shown. One representative experiment of 5 (Spl N and Spl T) or 7 (pLN and dLN) is depicted. Tumor sample 1 corresponds to one individual mouse. E, representative BV-8.1 CDR3 profiles of Treg cells obtained from naive and TC-1 tumor-bearing mice, in spleens, naive or tumor-dLNs, and tumors. BV-8.1 CDR3 profiles obtained from all 6 analyzed TC-1 tumor Treg samples are represented. Tumor samples 1 to 3 correspond to 3 individual mice experiments, whereas tumor samples 4 to 6 correspond to 3 independent sorting experiments using pooled tumors from 5 mice. F, landscape representation of BV-8.1 CDR3 profiles perturbations, compared with Treg cells obtained from naive spleen. FACS, fluorescence-activated cell sorting.

Published OnlineFirst May 9, 2012; DOI: 10.1158/0008-5472.CAN-12-0277

were expressed by less than 1% of the total Treg cell population (BV-5.1, BV-5.3, BV17, BV-18, and BV-19, Supplementary Fig. S5A). Some alterations in CDR3 peak distributions were observed for these BV families. However, this was due to the very low number of cells bearing these particular BV chains, which was insufficient for reproducible Gaussian distributions.

The CDR3 profiles of Treg cells from naive pLN or spleen in tumor-bearing mice also displayed Gaussian distributions that were very similar to those obtained with naive spleen samples (Fig. 2 and Supplementary Fig. S2E). No significant alteration in CDR3 profiles was observed for tumor dLN Treg cells (Fig. 2C).

In contrast, the CDR3 profiles of Tregs isolated from TC-1 tumors showed drastic alterations in all BV families (Fig. 2D and Supplementary Fig. S2F–H), leading to a non-Gaussian distribution. Several BV CDR3 profiles showed only 1 or 1 major CDR3 peaks often corresponding to 6 or 12 aa (amino acid). This contrasted with the usual 8 to 10 aa central CDR3 peaks found on bell-shaped distributions. CDR3 profile alterations were also observed in BV families expressed by a high percentage of tumor Treg cells. In addition, some BV families presenting altered CDR3 profiles have an increased percentage of usage in tumor Treg populations (i.e., BV-8.1: 12.4% in tumor sample 1 and 6.6% in tumor sample 2, vs. 3.4% in naive spleen samples, Supplementary Fig. S5A), which could reflect clonal expansions.

Biased BV-8.1 BJ usage by tumor Treg cells

Each CDR3 peak may represent hundreds or thousands of different sequences (21), each coding for a unique TCR with a particular antigen specificity. To determine whether the distortions observed for tumor Treg CDR3 profiles reflected clonal expansions of Treg cells, we analyzed the CDR3 sequences of Treg samples obtained from TC-1 tumor–bearing mice or from naive mice, prepared with identical cell numbers. We selected the BV-8.1 family for this analysis because biased CDR3 profiles—with a major 8-aa CDR3 peak—were observed in all of the tumor Treg samples analyzed (Fig. 2E). We used Gorochov mathematical analysis to quantify the distance between different CDR3 profiles by calculating the area beneath each peak (19). This showed that BV-8.1 CDR3 profiles of tumor Treg samples from 6 independent experiments were significantly different from those obtained with Treg samples from naive spleen or pLN or from tumor spleen and dLN (Fig. 2F).

To determine whether the perturbations observed in the BV-8.1 CDR3 profiles could result from biased *BJ* gene usage, we determined the percentage of usage of each *BJ* gene by BV-8.1–expressing Tregs. A significantly increased usage of BJ-2.5 was observed for tumor Treg samples versus naive pLN Treg cells, whereas the usage of BJ-2.3 and BJ-2.7 was markedly decreased (Supplementary Fig. S5B).

The existence of public sequences in the TCR repertoire of tumor-infiltrating Tregs suggests antigen-driven expansion

A total of 646 sequences were obtained from 6 different tumor Treg samples, and we analyzed the frequency of unique CDR3 sequence occurrence in these various samples (Supplementary Table S1). In naive pLN samples, only 17.3% of CDR3 sequences were present more than 3 times, and none of them was detected more than 6 times. In contrast, in tumor Treg samples, 37.9% of CDR3 sequences were present more than 3 times with 17.3% of these sequences detected more than 10 times.

To address whether these clonal expansions were driven by the recognition of the same antigen, we thus compared the BV-8.1 TCR sequences of Treg samples from tumors and tumor dLN with naive pLN samples from various independent experiments. First, we compared the pLN sequences from 2 naive mice (229 sequences for N1 and 324 sequences for N2). As expected, only one unique TCR amino acid sequence was shared by these 2 data sets (Table 1, top portion).

We applied the same methodology to compare every sequence from tumor Treg data sets with each other and with naive or tumor lymph node data sets. Unexpectedly, the percentages of shared sequences between the tumor Treg samples were extremely high, reaching a maximum of 67.3% of shared sequences between tumor samples 3 and 5 data sets (Table 1, top portion). In contrast, only 2 TCR aa sequences were common to the tumor and naive pLN data sets.

Three sequences were shared by all of the 6 tumor Treg samples analyzed and 3 other sequences were shared by 5 of the 6 tumor samples; all of these shared sequences were highly frequent (Table 1, bottom portion). These sequences correspond to the definition of public TCR sequences, involving a dominant immune response to a specific epitope present in most individuals (25). Furthermore, the 3 public sequences shared by all tumor samples only differed by a single amino acid and have a strong homology with 7 other tumor-shared sequences (Table 1, bottom portion). The high percentage of homology between these public sequences and the other shared sequences strongly suggests that an antigen-driven process underlies the clonal expansions of Treg cells expressing different TCR sequences with similar antigenic specificities. Most of these public sequences were also identified in dLN Tregs from tumor-bearing mice, but not in naive pLN Treg cells (Table 1, bottom portion). These findings imply that TAA recognition by Tregs, followed by clonal expansion, takes place within the tumor dLN before infiltrating the tumor tissue. For example, 77.7% of sequences from the tumor sample 2 Treg data set were also found in its corresponding dLN (Table 1, top portion). Moreover, these BV-8.1 CDR3 aa public sequences arise from different nucleic acid sequences, suggesting that this antigen-driven mechanism leads to activation of diverse and different Treg clones (Supplementary Table 2).

To confirm our results, we carried out a similar CDR3 sequence analysis with the BV-6 family for which several distortions were also observed in CDR3 spectratyping profiles of tumor Treg cell samples (Fig. 2D and Supplementary Fig. S2F-H). As previously shown for the BV-8.1 family, we observed a marked difference in the frequency of unique BV-6 CDR3 sequences obtained from tumor Treg samples versus tumor dLN and naive pLN (Supplementary Table S3). Several tumor Treg BV-6 CDR3 sequences were present at high frequencies; about 60% of unique CDR3 sequences were present at least 3 times. In contrast, most Treg BV-6 CDR3 sequences from tumor dLN and naive pLN were present only once or twice (82.5% and 79.2% of total sequences cloned, respectively). We then compared

Published OnlineFirst May 9, 2012; DOI: 10.1158/0008-5472.CAN-12-0277

Table 1. TC-1 tumor-infiltrating Treg cells share public sequences

Comparison of BV-8.1 TCR sequence data sets of Treg cells obtained from TC-1 tumors, tumor dLN, and naïve pLN[a]

		TC-1 Tumors						Tumor dLN		Naive pLN	
	Mouse	1	2	3	4	5	6	1	2	1	2
TC-1 Tumors	1		35.5	36.4	50.0	29.7	15.0	4.6	8.1	0.4	0.6
	2	6.7		16.4	35.1	20.7	9.8	4.3	20.0	0.9	0.6
	3	10.9	33.9		46.8	47.7	18.8	4.6	4.8	0.4	0.6
	4	21.2	33.1	41.8		38.7	21.8	7.2	5.2	0.4	0.9
	5	9.8	34.7	67.3	46.1		18.8	5.0	4.8	0.4	0.6
	6	9.3	29.8	34.5	46.8	31.5		4.8	5.2	0.4	0.6
Tumor dLN	1	9.3	42.1	18.2	49.4	24.3	17.3		8.5	0.9	4.3
	2	6.2	77.7	10.9	34.0	14.4	11.3	4.5		0.9	0.9
Naive pLN	1	1.6	12.4	3.6	9.1	3.6	0.8	0.9	1.1		0.3
	2	1.0	2.5	3.6	20.1	5.4	0.8	2.7	1.9	0.4	

BV-8.1 TCR aa public sequences shared by TC-1 tumor-infiltrating Treg samples[b]

CDR3 aa sequence	BJ	CDR3 length (aa)	Mouse	TC-1 Tumors 1	2	3	4	5	6	Tumor dLN 1	2	Naive pLN 1	2
SGTG**K**DTQ	2.5	8		2	3	2	30	6	1	10	4	0	2
SGTG**E**DTQ	2.5	8		3	14	2	14	4	1	4	2	1	0
SGTG**Q**DTQ	2.5	8		4	19	2	7	6	11	7	7	0	0
SGTG**D**DTQ	2.5	8		0	0	0	2	2	0	0	0	0	0
SGTG**R**DTQ	2.5	8		0	2	0	0	1	0	2	0	0	0
SG**R**G**Q**DTQ	2.5	8		3	4	2	3	6	0	1	0	0	0
SG**G**G**Q**DTQ	2.5	8		0	0	1	5	6	4	0	0	0	0
SG**Q**G**Q**DTQ	2.5	8		1	0	0	2	0	2	1	1	0	0
SG**L**G**Q**DTQ	2.5	8		1	0	0	0	0	0	0	6	0	0
TGTG**Q**DTQ	2.5	8		0	0	1	5	2	4	3	0	0	0
SG**L**G**E**DTQ	2.5	8		2	0	1	1	0	0	0	0	0	0
SG**Q**G**E**DTQ	2.5	8		3	0	1	2	2	3	2	0	0	0
S**A**GLGGYAEQ	2.1	10		3	9	1	10	4	0	0	0	0	0
S**V**GLGGYAEQ	2.1	10		0	2	0	1	0	0	0	0	0	0

[a]Samples were processed as in Fig. 2. Then, BV-8.1 TCR qPCR products were cloned and sequenced. The percentage of BV-8.1 TCR sequences, coding for the same amino acid sequences, between 2 samples was then calculated. The percentage of shared sequences between samples x and y is shown. $\%_{xy} = n_{(x\cap y)}/T_x$, in which $n_{(x\cap y)}$ equals the total number of clones from sample x coding for sequences also found on sample y. T_x = Total number of clones sequenced in sample x. x corresponds to the column in which the % is written: that is, the % of shared sequences between TC-1 tumors 1 and 2, 6.7% in column 1, line 2 correspond to $n_{(1\cap 2)}/T_1$ and 35.5% in column 2, line 1 = $n_{(2\cap 1)}/T_2$.
[b]BV-8.1 CDR3 amino acid sequences shared by at least 2 data sets from tumor Treg samples from 6 independent experiments. The corresponding *BJ* gene, CDR3 amino acid length, and number of clones sequenced coding for the indicated public sequence, found in each sample, are shown. Public sequences with only one amino acid of difference are presented in the same box. Amino acid sequence differences are indicated in bold and underlined.

the 5 different tumor Treg cell data sets as well as the tumor dLN and naive pLN data sets (Supplementary Table S4). As expected, none of the sequences from the tumor or tumor dLN samples was shared with the naive pLN data sets. Although less pronounced than the results obtained for the BV-8.1 family, we observed that different tumor Treg data sets, obtained from independent experiments, shared several sequences (Supplementary Table S4). Five public sequences were also identified

Published OnlineFirst May 9, 2012; DOI: 10.1158/0008-5472.CAN-12-0277

when analyzing these shared BV-6 CDR3 sequences from independent tumor Treg samples (Supplementary Table S5). These findings clearly confirmed our results obtained with the BV-8.1 family and support the hypothesis of an antigen-driven mechanism inducing Treg-cell infiltration of tumor tissue.

One of the BV-6 CDR3 public sequences was identical to one of the most represented BV-8.1 CDR3 public sequences. This strengthens the hypothesis that tumor Treg cells, even those expressing different BV families of receptors, could potentially be activated by the same antigens. As previously observed for the BV-8.1 family, there was a high percentage of shared sequences between the tumor and the tumor dLN; around 60% of BV-6 CDR3 sequences found in Tregs from tumor sample 2 were also found in the corresponding tumor dLN (Supplementary Table S4). These results supported the hypothesis that antigen recognition by Treg cells occurs within tumor dLN before expansion and migration into the tumor.

Tumor Teff cells show biased TCR repertoire

We next analyzed the TCR repertoire of intratumoral Teff cells to determine whether public sequences could also be detected for these cells. Foxp3$^-$CD4$^+$ T cells represented about 40% of tumor-infiltrating CD4$^+$ T cells (Fig. 1D). As expected, Teff cells, from either control spleen or pLN, displayed a more naive phenotype than Treg cells, characterized by high expression of CD62L and low expression of CD44 and CD69 markers (Supplementary Fig. S6A and B). In contrast, tumor-infiltrating Teff cells, displayed the phenotypic characteristic of activated cells.

For most BV, immunoscope profiles of tumor Teff cells presented severe distortions in CDR3 peak distribution (Fig. 3D and Supplementary Fig. S6C–F), characteristic of clonal expansions (Fig. 3E and F) when compared with the CDR3 profiles for naive spleen and pLN Teff samples (Fig. 3A and B).

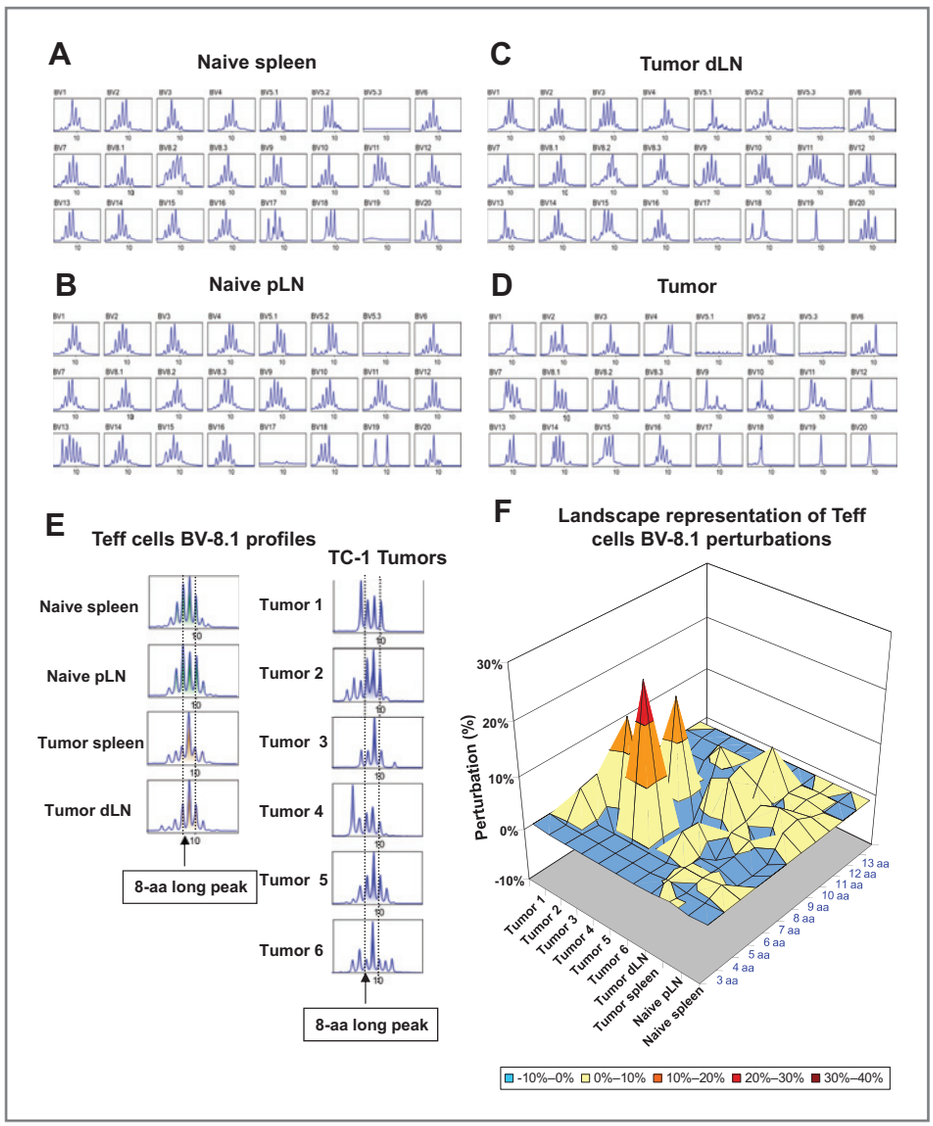

Figure 3. Immunoscope analysis reveals clonal expansions in TC-1 tumor-infiltrating Teff cells. Foxp3-GFP mice were injected on day 0 with 1×10^6 TC-1 cells. Twenty-five days later, mice were killed and tumors were processed to obtain cell suspensions. After AutoMacs CD4$^+$ cells enrichment, Foxp3-GFP$^-$ Teff cells were FACS sorted, and total RNA was purified and reverse transcribed. The corresponding cDNA material was then subject to quantitative PCR with primers specific to each BV family and resulting products were subjected to run-off reactions to obtain immunoscope profiles. CDR3 length profiles from FACS sorted CD4$^+$ Foxp3-GFP$^-$ Teff cells from naive spleen (7.6×10^4 cells; A), naive pLN (8.2×10^4 cells; B), tumor dLN (7.6×10^4 cells; C), and tumor (19×10^4 cells; D), sample 1. One representative experiment of 5 (Spl N and Spl T) and 7 (pLN and dLN) repeats is depicted. E, representative BV-8.1 CDR3 profiles of Teff cells obtained from naive and TC-1 tumor-bearing mice, in spleens, naive or tumor-dLNs, and tumors. BV-8.1 CDR3 profiles obtained from all 6 analyzed TC-1 tumor Teff samples are represented. Tumor samples 1 to 3 correspond to 3 individual mice experiments, whereas tumor samples 4 to 6 correspond to 3 independent sorting experiments using pooled tumors from 5 mice. F, landscape representation of BV-8.1 CDR3 profile perturbations compared with Teff cells obtained from naive spleen. FACS, fluorescence-activated cell sorting.

Published OnlineFirst May 9, 2012; DOI: 10.1158/0008-5472.CAN-12-0277

As for tumor Treg samples, the analysis of the frequency of unique TCR sequences identified in each sample revealed that several unique BV-8.1 and BV-6 TCR sequences were highly frequent in tumor Teff samples (Supplementary Tables S6 and S7). Analysis of BJ usage in BV-8.1 TCR sequences showed that TC-1 tumor Teff cells display a BJ usage similar to that in naive pLN Treg cells (Supplementary Fig. S5B). Only a significant increase BJ-1.3 usage by tumor Teff cells versus tumor and naive pLN Treg cells was observed.

We then compared the BV-8.1 sequences obtained from all tumor samples in 6 independent experiments. The percentage of BV-8.1 CDR3 sequences common to all of the 6 analyzed tumor Teff cell data sets was surprisingly low (Supplementary Table S8A). Only one TCR aa sequence, shared by 2 different tumor Teff data sets, could be detected (Supplementary Table S8B). Furthermore, no shared CDR3 sequences between the different data sets for tumor Teff cells could be identified when analyzing the BV-6 family (data not shown). Thus, although biased immunoscope profiles were observed and a high number of sequence copies were detected—confirming the existence of clonal expansions—the antigen-driven process governing tumor Teff infiltration seems to be more diverse and polyspecific than for tumor Treg cells.

Tumor Teff and Treg cells display distinct TCR repertoires

Conversion of Teffs into Tregs, by the expression of the transcription factor Foxp3, could explain the high percentage of intratumoral Treg cells. To test this hypothesis, we compared for each independent experiment tumor Teff and Treg BV-8.1 TCR sequences (Table 2). Only 5 aa TCR sequences were shared by these 2 populations, and each shared sequence was identified for a single tumor sample. In addition, none of the public sequences identified for tumor Treg samples could be detected on tumor Teff samples. Identical results were obtained when comparing BV-6 CDR3 sequences obtained from tumor Treg and Teff cells (Supplementary Table S9). Only two sequences were shared by these 2 populations in only one tumor sample and at a low number of copies. These data strongly suggested that conversion is not an active process responsible for the accumulation of Treg cells into tumor tissue.

Public sequences is a general feature of tumor-infiltrating Tregs

We next determined whether the oligoclonal and biased TCR repertoire observed for TC-1 tumor-infiltrating Treg cells is intrinsic to the TC-1 tumor model or is a general feature of tumor-infiltrating Treg cells. To do this, we carried

Table 2. Analysis of shared BV-8.1 TCR sequences between TC-1 tumor-infiltrating Treg and Teff cells

Total number of unique BV-8.1 TCR nucleic sequences found in both Treg and Teff data sets obtained from the same TC-1 tumor sample[a]

	TC-1 Tumors					
Mouse	**1**	**2**	**3**	**4**	**5**	**6**
Us	0	2	0	2	0	1
Treg Ts	0	40 (33.1)	0	2 (1.3)	0	1 (0.8)
Teff Ts	0	3 (2.6)	0	35 (26.1)	0	1 (0.8)
Total Seq compared	204	238	171	288	231	255

BV-8.1 CDR3 amino acid sequences shared by Treg and Teff data sets obtained from the corresponding TC-1 tumor sample[b]

	BJ	CDR3 length (aa)	Treg	Teff
Tumor 2				
SGTGEDTQ	2.5	8	17	2
SVQGRNSPL	1.6	9	23	1
Tumor 4				
GGAYEQ	2.7	6	1	34
STTGTYEQ	2.7	8	1	1
Tumor 6				
SDEGGQNTL	2.4	9	1	1

[a]Us, total number of unique sequences shared; Ts, total number of clones sequenced coding for these shared sequences, found in each T-cell subset. The corresponding percentage among total clones sequenced is shown in parentheses.

[b]The corresponding *BJ* gene, CDR3 amino acid length, and number of clones sequenced coding for the indicated sequences found in each sample are shown.

Published OnlineFirst May 9, 2012; DOI: 10.1158/0008-5472.CAN-12-0277

out a similar TCR repertoire analysis in the MO-5 tumor model, which is a melanoma cell line expressing OVA protein. MO-5 tumors were extensively infiltrated by Tregs, which represented about 45% of tumor-infiltrating CD4$^+$ T cells (Fig. 4A). As with the TC-1 model, tumor-infiltrating Treg cells displayed an activated phenotype characterized by complete downregulation of CD62L (Fig. 4B and Supplementary Fig. S7B).

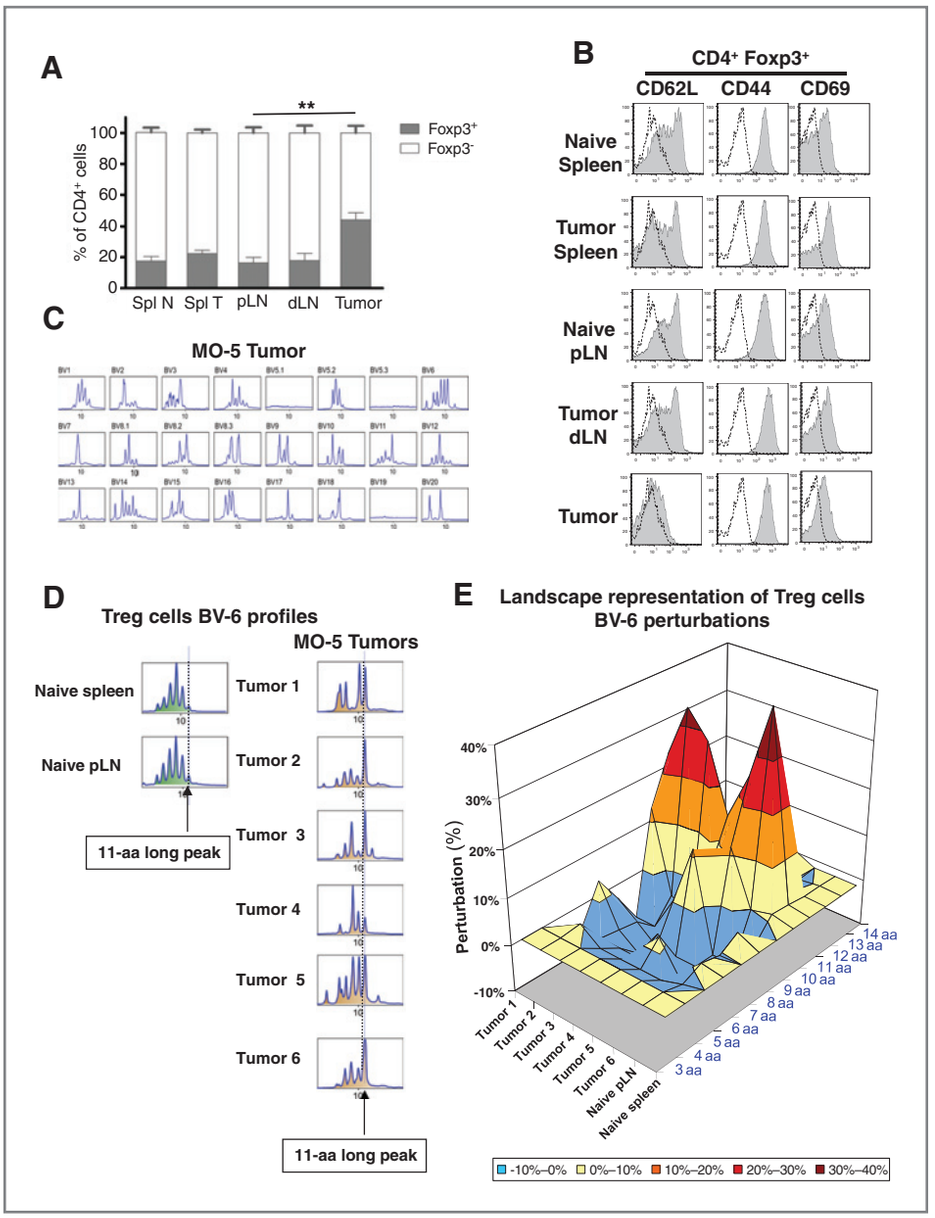

Figure 4. MO-5 tumors are infiltrated with high percentage of activated Treg cells. Foxp3-GFP mice were injected on day 0 with 5×10^5 MO-5 cells. Twenty days later, mice were killed and spleens, tumor-dLNs, and tumors were processed to obtain cell suspensions that were counted, stained, and analyzed by flow cytometry. Spleens and pLNs from naive Foxp3-GFP mice were identically processed and used as controls. A, percentage (mean $\pm$ SD) of CD45$^+$ CD3$^+$CD4$^+$ cells expressing Foxp3 after FACS analysis, gated on live cells. Results represent pooled data from 3 independent experiments, $n = 4$ (Spl N and Spl T), $n = 6$ (pLN, dLN and tumor). **, $P < 0.01$, as determined by one-way ANOVA. B, surface expression of CD62L, CD44, and CD69 molecules on CD4$^+$ Foxp3-GFP$^+$ Treg cells. Labelings with isotype control mAbs are represented with dashed lines. One representative experiment of 3 is depicted. C, after AutoMacs CD4$^+$ cells enrichment, Foxp3-GFP$^+$ Treg cells were FACS sorted, total RNA was purified, and reverse transcribed. The corresponding cDNA was subjected to quantitative PCR with primers specific to each BV family. The resulting products were then subjected to run-off reactions to obtain immunoscope profiles. The CDR3 length profiles from FACS sorted CD4$^+$Foxp3-GFP$^+$ Treg cells from one representative MO-5 tumor sample (3.2×10^4 cells, sample 1) is shown. D, representative BV-6 CDR3 profiles of Treg cells obtained from naive spleen and lymph nodes and from MO-5 tumors (samples 1–6) obtained from individual MO-5 tumor-bearing mice 20 days after the tumor graft. E, landscape representation of BV-6 CDR3 profiles perturbations compared with Treg cells obtained from naive spleen. FACS, fluorescence-activated cell sorting.

Published OnlineFirst May 9, 2012; DOI: 10.1158/0008-5472.CAN-12-0277

Immunoscope profiles from the various BV families presented severe distortions in CDR3 peak distributions (Fig. 4C and Supplementary Fig. S7C–E) in the 6 independently analyzed MO-5 tumors. BV-8.1 CDR3 sequencing revealed that several unique TCR sequences were present in high frequencies in MO-5 tumor Treg samples (Supplementary Table S10). None of the BV-8.1 CDR3 sequences identified in TC-1 Tregs—including the public sequences—were found in the data set for MO-5 tumor Treg samples (data not shown). MO-5 tumor Treg cells showed similar BJ usage compared with naive pLN Treg cells for most BJ families (Supplementary Fig. S5B). Only BJ-1.2 usage was increased in MO-5 tumor Treg cells compared with naive pLN Treg cells.

We then analyzed the CDR3 sequences from the BV-6 family that displayed biased CDR3 profiles in most of the MO-5 tumor Treg samples analyzed (Fig. 4C and Supplementary Fig. S7C–E) with one major CDR3 peak of 11 aa (Fig. 4D and E). Moreover, several unique BV-6 TCR sequences were present at very high frequency in MO-5 tumor Treg samples (Supplementary Table S11). Comparison of the BV-6 CDR3 data sets showed high percentages of shared sequences between the various MO-5 tumor Treg samples (Table 3, top portion). Analysis of these sequences revealed several public sequences shared by 2 to 4 of the 6 MO-5 tumor Treg samples (Table 3, middle, portion).

Finally, we compared BV-6 CDR3 sequences from TC-1 tumor Treg samples with those from MO-5 tumor Treg samples. Only one BV-6 CDR3 sequence was shared between both tumor models and was only present in 2 tumor samples (Table 3, bottom portion). This shared sequence corresponded to a 9-aa CDR3 sequence, whereas all public sequences found in the MO-5 tumor model were 11-aa CDR3 sequences.

Discussion

The infiltration of tumor tissue by Treg cells has been widely reported in human cancers and in murine tumor models (8, 9). However, the role played by this regulatory population in tumor tolerance/protection against immunotherapy remains unclear (26). Understanding the mechanisms by which Treg cells migrate and accumulate into the tumor tissue is of primary importance for the development of efficient immunotherapies.

We aimed to establish whether infiltration of tumor tissue by Tregs is due to either tumor inflammation promoting the migration and conversion of $CD4^+$ T cells into tumor tissue or to antigen-driven activation and expansion of Treg cells. To answer this question, we used the immunoscope technology to carry out a TCR repertoire diversity analysis of Treg and Teff populations in non-TCR–transgenic Foxp3-GFP knockin mice, bearing either TC-1 or MO-5 large solid tumors.

The immunoscope technology enables the global analysis of a complete TCR repertoire without the need for high-throughput sequencing. Analysis of CDR3 peak lengths distribution for each BV family is a good indicator of T-cell repertoire diversity. Gaussian-like distributions of CDR3 peak lengths suggest a diverse repertoire (21, 27). In contrast, distortions on CDR3 length profiles strongly indicate a biased repertoire due to clonal expansions. Such distortions have already been observed in allograft models (28) and chronic infections (19). Our study represents the first analysis of the complete TCR repertoire of $CD4^+$ T cells in non-TCR transgenic mice expressing or not expressing the Foxp3-GFP transcription factor, using 2 different solid tumor models.

The TCR repertoire of mouse Treg cells at steady state has been widely documented (29). Our present study shows that Treg cells from splenic or pLNs harbor a very diverse repertoire, with CDR3 spectratyping profiles showing Gaussian distributions in all BV families, confirming earlier reports (30). Treg CDR3 spectratyping profiles from the spleen or dLN from tumor-bearing mice showed no distortion and were comparable with those obtained from control samples. In agreement with other investigators, BV usage by Treg and Teff cells was similar (31). In contrast, TC-1 tumor-infiltrating Treg and Teff cells displayed CDR3 spectratyping profiles characteristic of biased and strongly perturbed repertoires, typical of clonal expansions, suggesting that strong T-cell responses have occurred within the tumor tissue.

We observed an extremely high percentage of overlapping sequences when comparing the sequence data sets for tumor-infiltrating Treg cells CDR3 BV-8.1 aa TCR obtained from different individuals and independent experiments. This identified common TCR sequences, called "public sequences." The observation of these public TCRs is related to a process known as clonal dominance, corresponding to the dominance of a particular clonotype over others involved in an immune response to a specific epitope. Venturi and colleagues hypothesized that public sequences result from a mechanism called convergent recombination, in which the TCR diversity generated by V-D-J recombination leads to the same or similar nucleotide sequences in some cases (25). We indeed showed that in the same individual, public TCR BV-8.1 sequences in tumor-infiltrating Treg cells shared the same amino acid sequence and were encoded by several distinct nucleic sequences. Most of these public TCR BV-8.1 sequences only differed by 1 or 2 amino acids, constituting consensus groups of amino acid motifs. Finally, not all of the public sequences observed within an individual correspond to one single clonotype expansion. This excludes the possibility that the sequence expansions we observed result from artifactual amplification.

In tumor-bearing mice, public sequences constituted a large percentage of CDR3 BV-8.1 TCR of intratumoral Treg cells, strongly suggesting that infiltration of tumor tissue by these cells after activation in the dLNs, following recognition of immunodominant antigens, is followed by an intense proliferation. This skews the initially highly diverse TCR repertoire toward a few dominant clones. This observation was not limited to the BV-8.1 family as public sequences and clonal expansions were also observed in the CDR3 aa TCR sequence data sets from the BV-6 family for tumor-infiltrating Treg cells.

In contrast with these results, no public sequences were observed in tumor-infiltrating Teff cells when analyzing BV-8.1 and BV-6 CDR3 sequences. However, CDR3 spectrotype distortions and clonal expansions were also detected in this T-cell subset. One possibility is that Teff cells that have recognized tumor cell antigens in the dLNs and have been recruited to the

Published OnlineFirst May 9, 2012; DOI: 10.1158/0008-5472.CAN-12-0277

Table 3. Comparison of BV-6 TCR sequence data sets of Treg cells obtained from MO-5 tumors

		MO-5 Tumors						Naive pLN
	Mouse	1	2	3	4	5	6	1
MO-5 Tumors	1		22.2	2.7	0	0	31.3	0
	2	13.3		61.3	0	26.6	8.1	0
	3	7.6	51.9		22.1	26.6	12.1	0
	4	0	0	9.0		0	4.0	0
	5	0	14.8	57.7	0		8.1	0
	6	5.7	14.8	66.7	22.1	26.6		0
Naive pLN	1	0	0	0	0	0	0	

% of shared TCR sequences

< 10	10–20	20–30	30–40	> 40

	BJ	CDR3 length (aa)	Mouse	MO-5 Tumors 1	2	3	4	5	6
SIWTG**L**SNERL	1.4	11		0	8	64	0	25	8
SIWTG**V**SNERL	1.4	11		6	0	0	0	0	31
SIGLGGGAETL	2.3	11		8	7	3	0	0	0
SIWTGVSAETL	2.3	11		0	0	10	19	0	4

	BJ	CDR3 length (aa)	Tumor Mouse	MO-5 6	TC-1 4
SILGDTGQL	2.2	9		8	1

NOTE: Top portion, Foxp3-GFP mice were injected on day 0 with 5×10^5 MO-5 cells and 20 days later, mice were killed and tumors were processed to obtain cell suspensions. After AutoMacs $CD4^+$ cells enrichment, Foxp3-GFP^+ Treg cells were FACS sorted, total RNA was purified and reverse transcribed. The corresponding cDNA material was then subjected to quantitative PCR with primers specific to each BV family. BV-6 TCR qPCR products were cloned and sequenced. Then, the percentage of BV-6 TCR sequences coding for the same amino acid sequences between 2 samples was calculated as described in Table 1. Middle portion, BV-6 CDR3 amino acid sequences shared by at least 2 data sets of Treg cells obtained from 6 MO-5 individual tumors, or (bottom portion) shared by data sets of Treg cells obtained from TC-1 and MO-5 tumors. The corresponding *BJ* gene, CDR3 amino acid length, and number of clones sequenced coding for the indicated sequence found in each sample are shown. Public sequences differing by only one amino acid are presented in the same box. Amino acid sequence differences are shown in bold and underlined.

tumor site became rapidly exhausted. Another possibility is that Teff cells—specific to TC-1 antigens—recognize a more diverse set of epitopes compared with Treg cells. Alternatively, the high percentage of overlapping TCR sequences of tumor-infiltrating Tregs cells could be due to a smaller size of the Treg repertoire as compared with Teff cells. Finally, in this study, we only analyzed 2 different BV families, and we cannot exclude the existence of Teff cells public sequences in other BV families.

Published OnlineFirst May 9, 2012; DOI: 10.1158/0008-5472.CAN-12-0277

It has been recently proposed that the rapid Treg recruitment and/or expansion into tumors is a consequence of early tumor cell recognition by memory Treg cells specific to self-antigens (10). To address whether the public sequences detected in TC-1 tumor-infiltrating Treg cells reflect the expansion of self-reactive clonotypes, we carried out a similar Treg TCR repertoire analysis in another tumor model, MO-5. As with the TC-1 model, we observed several distortions in the CDR3 spectrotype profiles of most BV families in the MO-5 tumor model. Public sequences were also detected in the BV-6 CDR3 TCR data sets obtained from MO-5 tumor-infiltrating Treg cells. However, only one BV-6 CDR3 TCR aa sequence was shared between MO-5 and TC-1 tumor-infiltrating Treg cells. The demonstration that different public sequences have been selected in the TC-1 and MO-5 models suggests a process involving the recognition of specific tumor antigens rather than a mechanism driven by the recognition of autoantigens. Whether the biologic properties of the E6 and E7 HPV oncoproteins expressed by TC-1 cells, compared with ovalbumin expressed by MO5 cells, could affect this process, remains to be determined.

Public $CD8^+$ T-cell responses have been reported in the case of chronic and persistent viral infections (32). In these studies, the demonstration of public TCR sequences was carried out in models in which a single or a few antigens are the main target of the immune system (33, 34). To our knowledge, this is the first demonstration of public TCR sequences dominating the intratumoral Treg repertoire. Most studies with regard to the TCR repertoire of $CD4^+$ T cells during the immune response to tumor have been carried out in TCR transgenic mice (35).

Two major subsets of Treg cells have been defined. Natural $CD4^+$ Treg cells arise from the thymus and harbor a strong Foxp3 expression and suppressor activity (4). Adaptive Treg cells are Foxp3-negative $CD4^+$ T cells that acquire Foxp3 expression and suppressive functions in the periphery after Ag exposure under particular conditions, a process known as conversion (36). The tumor microenvironment is considered to gather favorable conditions for conversion, such as inappropriate Ag presentation or high amounts of TGF-β (37, 38). To address whether conversion takes place in the TC-1 tumor model, we compared TCR BV-8.1 sequences obtained from tumor-infiltrating Treg and Teff cells from the same mice. Very few sequences were shared between Treg and Teff tumor-infiltrating T cells and none corresponded to public sequences. Although we cannot exclude the possibility that identical sequences could have been identified in other BV families, these data strongly suggest that conversion is not an active process at the tumor site, at least in TC-1 tumor model. These results are consistent with several TCR repertoire analysis studies that conclude that Treg conversion is a rare event, occurring at low frequency at steady state (30, 39, 40) or in carcinogen-induced tumors (41). However, one recent publication concluded that most Treg cells in tumors are likely generated by the conversion of effector $CD4^+$ T cells (35). This may be because the study used TCR^{mini} mice bearing B16 melanoma. Results obtained in a TCR transgenic mouse model could reflect biased observations due to the particular TCR specificity harbored by T cells.

Our study shows that a large proportion of tumor-infiltrating Treg sequences, especially those encoding public sequences, are found in the repertoire of Treg cells obtained from the dLNs. Treg cells may, therefore, be activated in the dLN, start their first round of proliferation, and then migrate to the tumor site, where they continue to proliferate and accumulate. However, an alternative scenario in which Tregs migrate from the tumors to lymphoid organs could not be excluded. Within the tumor site, clonal deletion or apoptosis of Teff cells may contribute to Treg cell expansion by allowing easier access to antigens. Alternatively, inside the tumor, Treg cells could accumulate by capturing IL-2 locally produced by activated Teff cells. Understanding the mechanisms promoting the expansion and survival of Treg inside the tumor and the antigens leading to clonal dominance and selection of public sequences is of primary importance to develop effective immunotherapy.

Disclosure of Potential Conflicts of Interest

No potential conflicts of interest were disclosed.

Authors' Contributions

Conception and design: A. Sainz-Perez, A. Lim, C. Leclerc
Development of methodology: A. Lim
Analysis and interpretation of data (e.g., statistical analysis, biostatistics, computational analysis): A. Sainz-Perez, A. Lim, B. Lemercier, C. Leclerc
Writing, review, and/or revision of the manuscript: A. Sainz-Perez, A. Lim, C. Leclerc
Administrative, technical, or material support (i.e., reporting or organizing data, constructing databases): A. Sainz-Perez, C. Leclerc
Study supervision: A. Sainz-Perez, C. Leclerc

Acknowledgments

The authors thank Pierre-Henri Commere for his excellent technical help in T-cell sorting.

Grant Support

This work was supported by grants from the Ligue Nationale Contre le Cancer (Equipe Labellisée 2011), Conseil Régional IdF/Cancéropôle IdF and Banque Privée Européenne. A. Sainz-Perez was supported by Association pour la Recherche sur le Cancer.

The costs of publication of this article were defrayed in part by the payment of page charges. This article must therefore be hereby marked *advertisement* in accordance with 18 U.S.C. Section 1734 solely to indicate this fact.

Received January 27, 2012; revised April 17, 2012; accepted April 30, 2012; published OnlineFirst May 9, 2012.

References

1. Sakaguchi S, Sakaguchi N, Asano M, Itoh M, Toda M. Immunologic self-tolerance maintained by activated T cells expressing IL-2 receptor alpha-chains (CD25). Breakdown of a single mechanism of self-tolerance causes various autoimmune diseases. J Immunol 1995;155:1151–64.
2. Fontenot JD, Gavin MA, Rudensky AY. Foxp3 programs the development and function of CD4+CD25+ regulatory T cells. Nat Immunol 2003;4:330–6.
3. Hori S, Nomura T, Sakaguchi S. Control of regulatory T cell development by the transcription factor Foxp3. Science 2003;299:1057–61.

Published OnlineFirst May 9, 2012; DOI: 10.1158/0008-5472.CAN-12-0277

4. Sakaguchi S. Naturally arising Foxp3-expressing CD25+CD4+ regulatory T cells in immunological tolerance to self and non-self. Nat Immunol 2005;6:345–52.
5. Shevach EM. Mechanisms of foxp3+ T regulatory cell-mediated suppression. Immunity 2009;30:636–45.
6. Belkaid Y. Regulatory T cells and infection: a dangerous necessity. Nat Rev Immunol 2007;7:875–88.
7. Nishikawa H, Sakaguchi S. Regulatory T cells in tumor immunity. Int J Cancer 2010;127:759–67.
8. Galon J, Costes A, Sanchez-Cabo F, Kirilovsky A, Mlecnik B, Lagorce-Pages C, et al. Type, density, and location of immune cells within human colorectal tumors predict clinical outcome. Science 2006;313:1960–4.
9. Curiel TJ, Coukos G, Zou L, Alvarez X, Cheng P, Mottram P, et al. Specific recruitment of regulatory T cells in ovarian carcinoma fosters immune privilege and predicts reduced survival. Nat Med 2004;10:942–9.
10. Darrasse-Jeze G, Bergot AS, Durgeau A, Billiard F, Salomon BL, Cohen JL, et al. Tumor emergence is sensed by self-specific CD44hi memory Tregs that create a dominant tolerogenic environment for tumors in mice. J Clin Invest 2009;119:2648–62.
11. Hsieh CS, Liang Y, Tyznik AJ, Self SG, Liggitt D, Rudensky AY. Recognition of the peripheral self by naturally arising CD25+ CD4+ T cell receptors. Immunity 2004;21:267–77.
12. Coombes JL, Siddiqui KR, Arancibia-Carcamo CV, Hall J, Sun CM, Belkaid Y, et al. A functionally specialized population of mucosal CD103+ DCs induces Foxp3 +regulatory T cells via a TGF-beta and retinoic acid-dependent mechanism. J Exp Med 2007;204:1757–64.
13. Sun CM, Hall JA, Blank RB, Bouladoux N, Oukka M, Mora JR, et al. Small intestine lamina propria dendritic cells promote *de novo* generation of Foxp3 T reg cells via retinoic acid. J Exp Med 2007;204:1775–85.
14. Pannetier C, Cochet M, Darche S, Casrouge A, Zoller M, Kourilsky P. The sizes of the CDR3 hypervariable regions of the murine T-cell receptor beta chains vary as a function of the recombined germ-line segments. Proc Natl Acad Sci U S A 1993;90:4319–23.
15. Wang Y, Kissenpfennig A, Mingueneau M, Richelme S, Perrin P, Chevrier S, et al. Th2 lymphoproliferative disorder of LatY136F mutant mice unfolds independently of TCR-MHC engagement and is insensitive to the action of Foxp3+ regulatory T cells. J Immunol 2008;180:1565–75.
16. Lin KY, Guarnieri FG, Staveley-O'Carroll KF, Levitsky HI, August JT, Pardoll DM, et al. Treatment of established tumors with a novel vaccine that enhances major histocompatibility class II presentation of tumor antigen. Cancer Res 1996;56:21–6.
17. Lim A, Baron V, Ferradini L, Bonneville M, Kourilsky P, Pannetier C. Combination of MHC-peptide multimer-based T cell sorting with the Immunoscope permits sensitive *ex vivo* quantitation and follow-up of human CD8+ T cell immune responses. J Immunol Methods 2002;261:177–94.
18. Arden B, Clark SP, Kabelitz D, Mak TW. Human T-cell receptor variable gene segment families. Immunogenetics 1995;42:455–500.
19. Gorochov G, Neumann AU, Kereveur A, Parizot C, Li T, Katlama C, et al. Perturbation of CD4+ and CD8+ T-cell repertoires during progression to AIDS and regulation of the CD4+ repertoire during antiviral therapy. Nat Med 1998;4:215–21.
20. Arstila TP, Casrouge A, Baron V, Even J, Kanellopoulos J, Kourilsky P. A direct estimate of the human alphabeta T cell receptor diversity. Science 1999;286:958–61.
21. Casrouge A, Beaudoing E, Dalle S, Pannetier C, Kanellopoulos J, Kourilsky P. Size estimate of the alpha beta TCR repertoire of naive mouse splenocytes. J Immunol 2000;164:5782–7.
22. Yousfi Monod M, Giudicelli V, Chaume D, Lefranc MP. IMGT/JunctionAnalysis: the first tool for the analysis of the immunoglobulin and T cell receptor complex V-J and V-D-J JUNCTIONs. Bioinformatics 2004;20 Suppl 1:i379–85.
23. IMGT. Available from: http://www.imgt.org/IMGT_vquest/share/textes/imgtvquest.html.
24. Berraondo P, Nouze C, Preville X, Ladant D, Leclerc C. Eradication of large tumors in mice by a tritherapy targeting the innate, adaptive, and regulatory components of the immune system. Cancer Res 2007;67:8847–55.
25. Venturi V, Price DA, Douek DC, Davenport MP. The molecular basis for public T-cell responses? Nat Rev Immunol 2008;8:231–8.
26. Zou W. Regulatory T cells, tumour immunity and immunotherapy. Nat Rev Immunol 2006;6:295–307.
27. Cibotti R, Cabaniols JP, Pannetier C, Delarbre C, Vergnon I, Kanellopoulos JM, et al. Public and private V beta T cell receptor repertoires against hen egg white lysozyme (HEL) in nontransgenic versus HEL transgenic mice. J Exp Med 1994;180:861–72.
28. Guillet M, Brouard S, Gagne K, Sebille F, Cuturi MC, Delsuc MA, et al. Different qualitative and quantitative regulation of V beta TCR transcripts during early acute allograft rejection and tolerance induction. J Immunol 2002;168:5088–95.
29. Pacholczyk R, Kern J. The T-cell receptor repertoire of regulatory T cells. Immunology 2008;125:450–8.
30. Pacholczyk R, Ignatowicz H, Kraj P, Ignatowicz L. Origin and T cell receptor diversity of Foxp3+CD4+CD25+ T cells. Immunity 2006;25:249–59.
31. Romagnoli P, Hudrisier D, van Meerwijk JP. Preferential recognition of self antigens despite normal thymic deletion of CD4(+)CD25(+) regulatory T cells. J Immunol 2002;168:1644–8.
32. Davenport MP, Price DA, McMichael AJ. The T cell repertoire in infection and vaccination: implications for control of persistent viruses. Curr Opin Immunol 2007;19:294–300.
33. Fourcade J, Sun Z, Kudela P, Janjic B, Kirkwood JM, El-Hafnawy T, et al. Human tumor antigen-specific helper and regulatory T cells share common epitope specificity but exhibit distinct T cell repertoire. J Immunol 2010;184:6709–18.
34. Serana F, Sottini A, Caimi L, Palermo B, Natali PG, Nistico P, et al. Identification of a public CDR3 motif and a biased utilization of T-cell receptor V beta and J beta chains in HLA-A2/Melan-A-specific T-cell clonotypes of melanoma patients. J Transl Med 2009;7:21.
35. Kuczma M, Kopij M, Pawlikowska I, Wang CY, Rempala GA, Kraj P. Intratumoral convergence of the TCR repertoires of effector and Foxp3+ CD4+ T cells. PLoS One 2010;5:e13623.
36. Bluestone JA, Abbas AK. Natural versus adaptive regulatory T cells. Nat Rev Immunol 2003;3:253–7.
37. Chen W, Jin W, Hardegen N, Lei KJ, Li L, Marinos N, et al. Conversion of peripheral CD4+CD25- naive T cells to CD4+CD25+ regulatory T cells by TGF-beta induction of transcription factor Foxp3. J Exp Med 2003;198:1875–86.
38. Apostolou I, Verginis P, Kretschmer K, Polansky J, Huhn J, von Boehmer H. Peripherally induced Treg: mode, stability, and role in specific tolerance. J Clin Immunol 2008;28:619–24.
39. Lathrop SK, Santacruz NA, Pham D, Luo J, Hsieh CS. Antigen-specific peripheral shaping of the natural regulatory T cell population. J Exp Med 2008;205:3105–17.
40. Hsieh CS, Zheng Y, Liang Y, Fontenot JD, Rudensky AY. An intersection between the self-reactive regulatory and nonregulatory T cell receptor repertoires. Nat Immunol 2006;7:401–10.
41. Hindley JP, Ferreira C, Jones E, Lauder SN, Ladell K, Wynn KK, et al. Analysis of the T-cell receptor repertoires of tumor-infiltrating conventional and regulatory T cells reveals no evidence for conversion in carcinogen-induced tumors. Cancer Res 2011;71:736–46.

Published OnlineFirst May 9, 2012; DOI: 10.1158/0008-5472.CAN-12-0277

Cancer Research
The Journal of Cancer Research (1916–1930) | The American Journal of Cancer (1931–1940)

AACR American Association for Cancer Research

The T-cell Receptor Repertoire of Tumor-Infiltrating Regulatory T Lymphocytes Is Skewed Toward Public Sequences

Alexander Sainz-Perez, Annick Lim, Brigitte Lemercier, et al.

Cancer Res 2012;72:3557-3569. Published OnlineFirst May 9, 2012.